J Nanopart Res (2011) 13:5507–5517
DOI 10.1007/s11051-011-0538-1

RESEARCH PAPER

High-temperature redistribution of cation vacancies and irreversible magnetic transitions in the $Fe_{1-x}S$ nanodisks observed by the Mössbauer spectroscopy and magnetic measurements

Igor S. Lyubutin · Chun-Rong Lin · Shin-Zong Lu · Yu-Jhan Siao · Yuriy V. Korzhetskiy · Tatyana V. Dmitrieva · Yuliya L. Dubinskaya · Vyacheslav S. Pokatilov · Anastasiya O. Konovalova

Received: 5 March 2011 / Accepted: 29 July 2011 / Published online: 17 August 2011

Abstract The hexagonal pyrrhotite $Fe_{1-x}S$ nanodisks with the NiAs-type structure were synthesized by thermal decomposition of ferrous chloride and thiourea in oleylamine. The Mössbauer spectroscopy and magnetic measurements data indicate that a mixture of antiferromagnetic (AFM) and ferrimagnetic (FRM) phases with the NC ($N \geq 3$) and 2C-type superstructures is present in the $Fe_{1-x}S$ compound at temperatures between 80 K and Néel temperature T_N. At $T < 370$ K, the AFM phase prevails over the FRM phase. At $T > 370$ K, a redistribution of iron vacancies takes place, and the vacancy ordering transforms from the NC ($N \geq 3$) to 2C-type which essentially increases the magnetization with maximum value at 470 K. Heating the sample above the Néel temperature 565 K leads to a random distribution of vacancies, and this state is quenched upon subsequent cooling of the sample to 300 K. This gives rise to a pure AFM structure with a zero magnetic moment due to a total compensation of the moments in neighboring iron layers. Thus, the high-temperature redistribution of cation vacancies leads to irreversible magnetic transformations in the $Fe_{1-x}S$ nanoparticles.

Keywords Nanosheets · Pyrrhotite · Vacancy distribution · Mössbauer effect

I. S. Lyubutin (✉) · Y. V. Korzhetskiy · T. V. Dmitrieva · Y. L. Dubinskaya
Shubnikov Institute of Crystallography, Russian Academy of Sciences, Leninsky Av. 59, Moscow, Russia 119333
e-mail: lyubutin@ns.crys.ras.ru

C.-R. Lin (✉) · S.-Z. Lu · Y.-J. Siao
Institute of Nanotechnology and Department of Mechanical Engineering, Southern Taiwan University, No. 1 Nan-Tai Street, Yungkang Dist., Tainan City 710, Taiwan, ROC
e-mail: crlin@mail.stut.edu.tw; crlinspin@gmail.com

V. S. Pokatilov · A. O. Konovalova
Moscow Institute of Radio-Electronics and Automatics, Moscow, Russia 117454

Introduction

Iron sulfides $Fe_{1-x}S$ have a substantial deficiency at the iron sites, and at room temperature the stable phases are Fe_7S_8, Fe_9S_{10}, $Fe_{10}S_{11}$, $Fe_{11}S_{12}$, and FeS (Nakazawa and Morimoto 1971). The cation-deficient $Fe_{1-x}S$ materials have interesting magnetic properties, and can find a potential application in the nonvolatile phase-change magnetic memory devices (Takayama and Takagi 2006). The compounds $Fe_{1-x}S$ with $0 \leq x \leq 0.125$, extending from the nearly stoichiometric hexagonal troilite $Fe_{1-x}S$ ($0 \leq x \leq 0.05$) to the monoclinic Fe_7S_8 ($x = 0.125$), have the NiAs-like crystal structures, and belong to the so called pyrrhotite group (Wang and Salveson 2005). The clustering of Fe atoms in the troilite phase and the ordering of Fe atoms and cation vacancies in the more Fe-deficient compositions

lead to the superstructures. The troilite has a $2C$ superstructure of NiAs with the hexagonal lattice parameters $a = \sqrt{3}A$, $c = 2C$, where A and C are the axes of the NiAs subcell. The appearance of vacancies reduces the symmetry of the system from hexagonal to monoclinic. The monoclinic pyrrhotite Fe_7S_8 has a $4C$ superstructure of NiAs-type which can be represented as a derivative from FeS by subtraction of one Fe per eight FeS units (Wang and Salveson 2005; Bertaut 1953). The resultant structure is composed of the Fe sites layers separated by the S layers from the layers containing the Fe sites and the cation vacancies. As to magnetic properties, the $Fe_{1-x}S$ compounds can be antiferromagnetic (AFM) and/or ferrimagnetic (FRM), and the magnetic behavior is strongly dependent on composition and temperature (Wang and Salveson 2005; Lotgering 1956; Zapletal 1969; Marusak and Mulay 1979, 1980; Fei et al. 1995; Li and Franzen 1996).

In this article, we present the structural and magnetic properties of the newly synthesized iron sulfide nanosheets with a NiAs-like crystal structure studied by the Mössbauer spectroscopy and magnetic measurements in a wide temperature range 78–700 K. An evidence of the vacancy redistribution over iron layers, changing essentially the magnetic properties of the compound, was established at high-temperatures. We examined the inter- and intra-exchange interactions between Fe atoms taking into account the geometry of the exchange bonds, and found a model of the vacancy redistribution which explains the magnetic anomaly observed in the experiment.

Sample preparation and characterization

The nanoparticles of iron sulfide $Fe_{1-x}S$ were synthesized by thermal decomposition of the mixture of iron-oleylamine (Fe-OLA) complexes and sulfur-oleylamine (S-OLA) in a three-neck flask equipped with an inlet of argon gas, condenser, magnetic stirrer, thermocouple, and heating mantle. The details of the process are described in the previous studies (Lin et al. 2009, 2010) and summarized in Table 1.

The crystal structure and phase purity of the samples were examined by X-ray powder diffraction (XRD). As shown in Fig. 1, all reflections can be readily indexed to the hexagonal phase with NiAs-type structure ($P6_3/mmc$). An estimation of the crystallite size by the Scherrer's formula of the peak broadening (Langford and Wilson 1978) gives an average size $\sim$30.5 nm.

The particles shape and size were examined by the scanning electron microscope (SEM) and transmission electron microscope (TEM). The SEM images (Fig. 2a) show the aggregative plate-like particle structure with the thickness of the sheets about 30–50 nm. The TEM images (Fig. 2b–d) display particles with the accurate shape of hexagonal plates whose characteristic size is about 200–400 nm in plane and about 30–50 nm in thickness.

The Mössbauer spectroscopy and magnetic measurement data

The Mössbauer spectroscopy was applied to examine the phase composition, structural, and magnetic properties of the nanoparticles. The ^{57}Fe-Mössbauer spectra were recorded at temperatures between 80 and 700 K in the transmission geometry with a standard spectrometer operating in the constant accelerations regime. The gamma-ray source ^{57}Co(Rh) was at room temperature, and the isomer shifts were measured relative to metal α-Fe at room temperature. To exclude the sample oxidation, the

Table 1 Some details of the synthesis of the iron sulfide $Fe_{1-x}S$ nanoparticles. Fe-OLA ≡ iron-oleylamine complexes, S-OLA ≡ sulfur-oleylamine complexes, and Fe/S ≡ molar ratio of iron chloride tetrahydride ($FeCl_2{\cdot}4H_2O$) to thiourea (NH_2CSNH_2), $0 \le x \le 0.125$

No.	Sample's name	Composition	Structure	Fe/S	Synthesis (Lin et al. 2010)
1	FS-NA1	$Fe_{1-x}S$	NiAs-type	1/2	Fe-OLA + S-OLA → 180 °C, 2 h → 280 °C, 2 h
2	FS-NA2	$Fe_{1-x}S$	NiAs-type	1/1	Fe-OLA + S-OLA → 180 °C, 2 h → 280 °C, 2 h
3	FS-NA 3	$Fe_{1-x}S$	NiAs-type	1/3	Fe-OLA + S-OLA → 180 °C, 2 h → 280 °C, 2 h
4	FS-NA 4	$Fe_{1-x}S$	NiAs-type	1/4	Fe-OLA + S-OLA → 180 °C, 2 h → 280 °C, 2 h
5	FS-NA 5	$Fe_{1-x}S$	NiAs-type	1/5	Fe-OLA + S-OLA → 180 °C, 2 h → 280 °C, 2 h

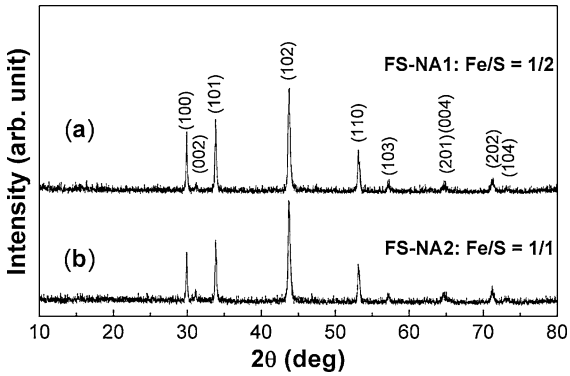

Fig. 1 Room temperature X-ray diffraction patterns of the $Fe_{1-x}S$ nanodisks recorded for the samples prepared at Fe/S = 1/2 (FS-NA1) and Fe/S = 1/1 (FS-NA2) conditions. Fe/S is the molar ratio of $FeCl_2{\cdot}4H_2O$ to NH_2CSNH_2. The reflection indexes correspond to the hexagonal NiAs-type structure ($P6_3/mmc$)

high-temperature measurements were performed in the vacuum and/or in argon filled furnaces.

We found that the room temperature Mössbauer spectra of all five samples prepared at different molar ratio of $FeCl_2{\cdot}4H_2O$ to NH_2CSNH_2 (see Table 1) are very similar. This supports the NiAs-type structure and implies similar magnetic behavior of the $Fe_{1-x}S$ nanoparticles in all the samples. The FS-NA1 and FS-NA2 samples (see Table 1) were investigated in a wide temperature range, and several Mössbauer spectra recorded at different temperatures are shown in Fig. 3. The magnetic splitting of spectra lines is gradually reduced as temperature increases from 80 to 570 K, and above 565 K the spectra transforms into a doublet typical of the paramagnetic state.

The spectra-line shape indicates that iron ions occupy several nonequivalent sites which can be explained by the presence of cation vacancies. We have examined several models of the spectra fitting, including plotting the distribution functions for the hyperfine parameters by the DISTRY program (Rusakov 2000), and found that the best fit can be obtained with four six-line components (shown in Fig. 4a, b) which relate to four nonequivalent iron sites. At room temperature, the values of isomer shifts (δ) for four components are in the range of 0.70–0.64 mm/s (Table 2), which shows that iron ions in all nonequivalent sites are in the valence state close to Fe^{2+}, and the trivalent iron does not appear in our $Fe_{1-x}S$ pyrrhotite. At 80 K, the values of the magnetic hyperfine fields H_{hf} for four Mössbauer components are about 335, 310, 279, and 245 kOe, and at room temperature, these values are reduced to 300, 280, 260, and 232 kOe, respectively. The values of all hyperfine parameters are given in Table 2.

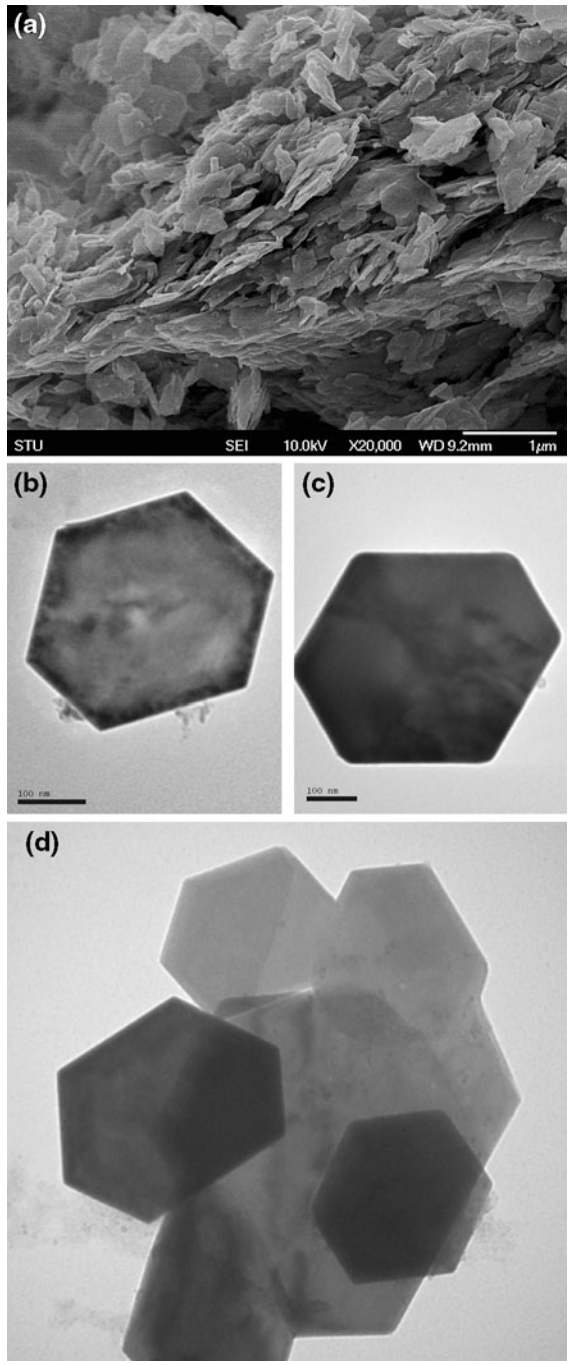

Fig. 2 SEM (**a**) and TEM (**b**, **c**, and **d**) images of the $Fe_{1-x}S$ nanoparticles

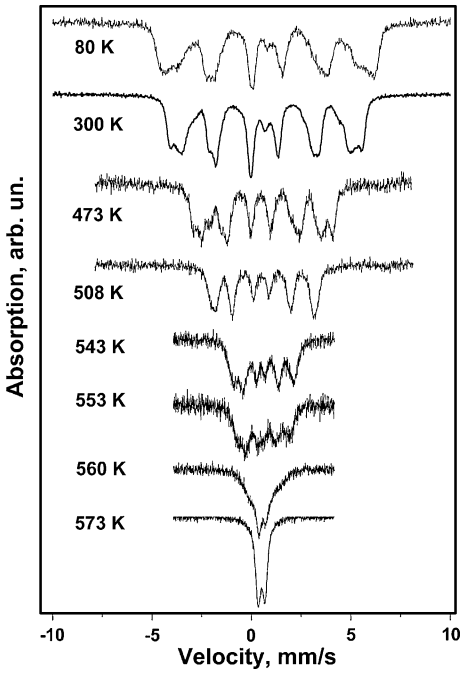

Fig. 3 The ^{57}Fe-Mössbauer spectra of $Fe_{1-x}S$ nanoparticles (FS-NA1) at different temperatures

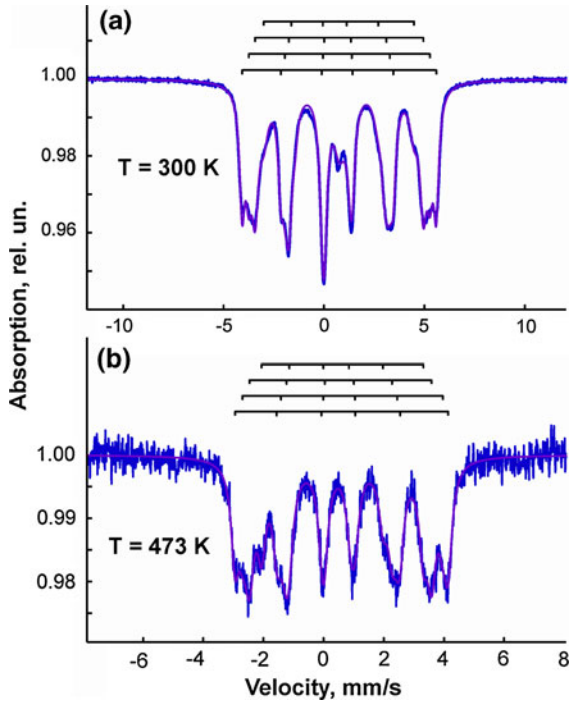

Fig. 4 The ^{57}Fe-Mössbauer spectra of $Fe_{1-x}S$ nanoparticles at temperatures 300 K (**a**) and 473 K (**b**). The spectra fitting to four magnetic components attributed to nonequivalent iron sites are shown by *grid-ticks* above the spectra. *Solid* (*color red*) *lines* correspond to the calculated spectra (Color figure online)

The temperature dependences of the hyperfine fields H_{hf} for three most intensive Mössbauer components are shown in Fig. 5. From the field behavior, we estimated the value of Néel temperature to be about 565 K. We found that the relative intensities of the Mössbauer components for nonequivalent iron sites change with the temperature increase from 400 to 550 K in accordance with the magnetic properties change. Above the Néel temperature, the Mössbauer spectrum consists of a broad doublet (Fig. 3) which can be related to several overlapping components in the paramagnetic state.

The magnetic measurements of the $Fe_{1-x}S$ nanoparticles were performed at temperatures between 300 and 700 K using the VSM-type magnetometer with the sample kept in the argon atmosphere. The hysteresis loops were measured at temperatures $300 \leq T \leq 650$ K in an applied field sweeping from -11 to 11 kOe. We found that upon heating, the magnetization value M is rather low in the region 300–370 K, and then it increases essentially and reaches maximum at 470 K (Fig. 6a). The peak-like transition in $M(T)$ starts at $\sim$370 K and ends near $\sim$560 K. Above 360 K, the hysteresis loops are typical of a ferromagnet, and the coercivity rises rapidly reaching a maximum value at 390 K, and then it decreases slowly showing a local maximum at 465 K (Fig. 6b).

Discussions

The interlayer and intralayer exchange interactions

The nonequivalent iron sites in the cation-deficient $Fe_{1-x}S$ compounds appear due to the presence of cation vacancies in the nearest neighboring of Fe ions. In the NiAs-type structure of $Fe_{1-x}S$, the Fe cations are octahedrally coordinated by six S anions (the FeS_6 octahedra) (Fig. 7), and the coordination polyhedron of S is the trigonal prism created by six Fe (the SFe_6 prisms) (Goodenough 1963; Wolf and Dwight 1993). Within the iron layers, the direct Fe–Fe ferromagnetic interactions J_1 connect the Fe ion with six nearest Fe neighbors (Fig. 7), but the Fe–Fe interionic distances are very large ($\sim$3.4 Å) and the

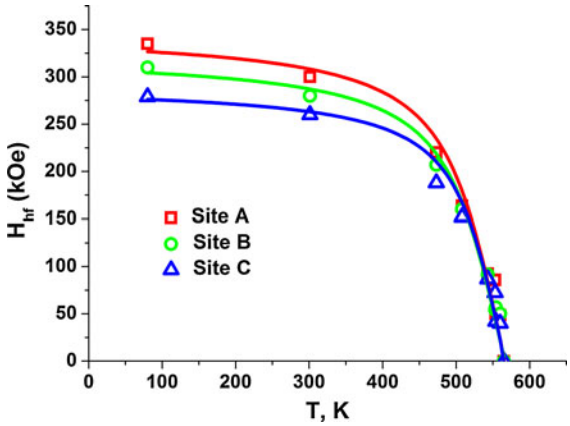

Fig. 5 The temperature dependences of the magnetic hyperfine field H_{hf} at the ^{57}Fe nuclei for three most intensive Mössbauer components in the $Fe_{1-x}S$ nanoparticles

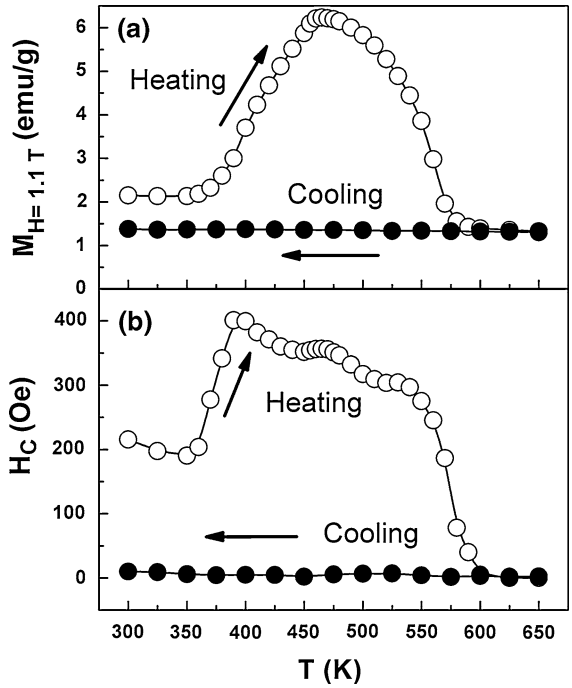

Fig. 6 Temperature dependence of magnetization $M_{H=1.1T}$ (**a**) and coercivity H_C (**b**) obtained from hysteresis loops of $Fe_{1-x}S$ nanoparticles

J_1 exchange interaction integral should be very small (Goodenough 1963). However, beside the direct interactions, the Fe ion is connected with 6 nearest Fe neighbors of the same layer by 12 superexchange Fe–S–Fe interactions J_2, which involve three sulfur ions above and three sulfur ions below the iron layer (Fig. 7). The angle of these Fe–S–Fe bonds is about 96° and the Fe–S distances are near 2.44 Å (Wolf and Dwight 1993). The 90° superexchange Fe–S–Fe interactions are supposed to be ferromagnetic ($J_2 > 0$) (Goodenough 1963).

The interlayer superexchange Fe–S–Fe interactions connect each Fe ion with 18 Fe ions from two nearest layers (nine bonds above and nine bonds below the selected Fe-layer), however, not all these bonds are equivalent (Fig. 7). Although the length of all Fe–S bonds is nearly the same ($\sim$2.44 Å), only 12 of the 18 bonds have the Fe–S–Fe bond angle of about 129° which is effective for the AFM interaction ($J_3 < 0$), while six interlayer bonds (J_4) are at the angle $\sim$62° (Fig. 7) which is not effective in the electronic d–p interaction (Goodenough 1963).

Table 2 Hyperfine parameters obtained from the ^{57}Fe-Mössbauer spectra at different temperatures for the nonequivalent iron sites in the $Fe_{1-x}S$ nanosheets: H_{hf} is the magnetic hyperfine field at ^{57}Fe nuclei, δ is the isomer shift relative to α-Fe at room temperature, ε is the quadrupole shift, S is the relative line area of the spectrum component, and Γ is the half-maximum line width

Spectra components	δ (mm/s) (±0.005)	ε (mm/s) (±0.005)	H_{hf} (kOe) (±2)	S (%) (±1.5)	Γ (mm/s) (±0.015)
$T = 300$ K					
Site-A($12J_3$)	0.701	0.105	300	26.2	0.315
Site-B($11J_3$)	0.711	0.098	280	23.6	0.383
Site-C($10J_3$)	0.716	0.076	260	34.0	0.411
Site-D($8J_3$)	0.636	0.206	232	16.3	0.549
$T = 473$ K					
Site-A($12J_3$)	0.545	0.109	220	25.2	0.302
Site-B($11J_3$)	0.576	0.117	207	17.2	0.376
Site-C($10J_3$)	0.543	0.041	188	33.9	0.375
Site-D($8J_3$)	0.523	0.209	167	23.7	0.345

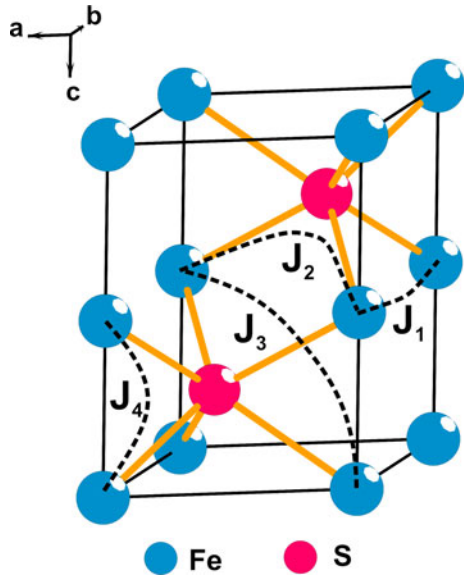

Fig. 7 The unit cell of the NiAs-type crystal structure of $Fe_{1-x}S$ compound. *Black* (*color blue*) *balls* are the Fe cations and *grey* (*color red*) *balls* are the S anions. The intralayer direct Fe–Fe and 90°-superexchange Fe–S–Fe bonds are shown by *dash lines* with J_1 and J_2, respectively, and the interlayer 129°- and 62°-superexchange Fe–S–Fe bonds are shown by *dash lines* with J_3 and J_4, respectively (Color figure online)

Here we note that the previous considerations of the Mössbauer and magnetic data of $Fe_{1-x}S$ on the basis of the 18 equivalent superexchange bonds were not correct (Levinson and Treves 1968; Ok and Lee 1973; Kim et al. 2009).

Nonequivalent iron sites

It is supposed that the magnetic structure of $Fe_{1-x}S$ consists of the ferromagnetic Fe layers in the *c* plane with an AFM coupling of the neighboring layers along the *c* axis (Lotgering 1956; Levinson and Treves 1968; Ok and Lee 1973, 1984; Kim et al. 2009; Ok et al. 1982). An appearance of the cation vacancies □ influences both the direct Fe–Fe and the superexchange Fe–S–Fe interactions. In general, the vacancies can be distributed randomly or orderly. In the layered NiAs structure, several types of the nonequivalent iron sites can be considered in the case of vacancy ordering (see Fig. 8a, b):

(1) The Site-1 exists in some local sites of a selected Fe-layer where there are not any vacancies

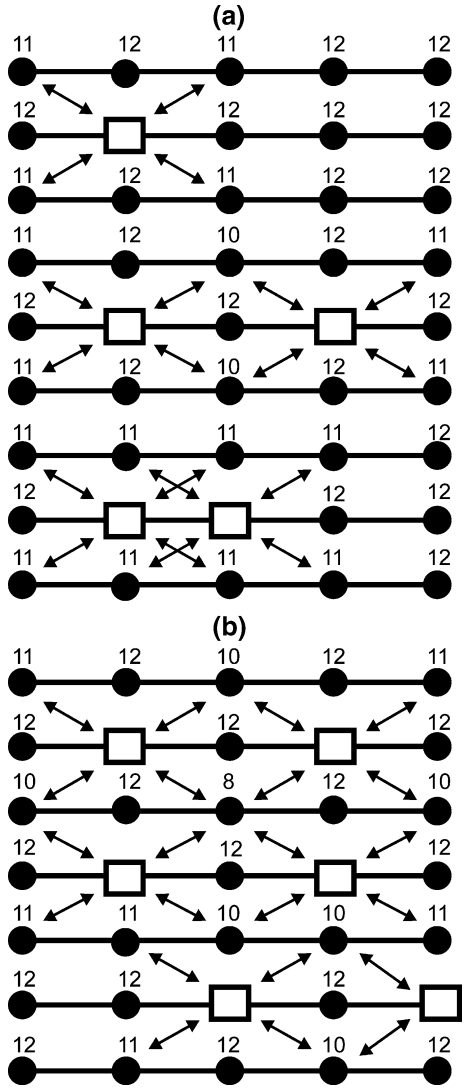

Fig. 8 Iron layers (*black balls*) stacked along the *c*-axis in the NiAs-type crystal structure of $Fe_{1-x}S$ compound. Schematic location of cation vacancies □ is shown for the cases of 3*C*-type (**a**) and 2*C*-type (**b**) of the vacancy ordering. Numerals at iron cations indicate the number of the interlayer 129°-superexchange Fe–S–Fe bonds J_3 of this cation with the iron ions from neighboring layers. *Arrows* show the broken J_3 bonds. Sulfur anions are not shown

(in the nearest environment of some Fe sites) both in this layer and in the two nearest layers above and below the selected layer (Fig. 8a). All the intralayer and interlayer (Fe–Fe and Fe–S–Fe) bonds are preserved in this case, and the magnetic state of the iron ions is governed by the $(6J_1 + 12J_2 + 12J_3)$

couplings. Only this type of sites should be presented in the stoichiometric FeS compound.

(2) The Sites-2 appears when the cation vacancies are in the selected Fe-layer, but there are not any vacancies in two nearest layers above and below the selected layer (Fig. 8a). In this case, vacancies can appear in each third (or in more distant) iron layer along the *c*-axis, and this type of the vacancies ordering we attribute to the N*C* superstructure with $N \geq 3$. The intralayer direct Fe–□ and 90°-superexchange Fe–S–□ bonds appear in this case but all interlayer Fe–S–Fe bonds are preserved. The magnetic state of the Fe ion having one nearest vacancy in the Site-2 is governed by the $(5J_1 + 10J_2 + 12J_3)$ coupling (Fig. 8a). Two in-layer vacancies would lead to the $(4J_1 + 8J_2 + 12J_3)$ coupling (Fig. 8a).

(3) The Sites-3 appears when there are not any vacancies in the selected Fe-layer, but the vacancies are located in one nearest layer above or below the selected layer (Fig. 8a). In this case, all in-layer Fe–Fe and Fe–S–Fe bonds are preserved and the interlayer Fe–S–□ bonds with one neighboring layer containing vacancies appear. This type of the vacancy ordering corresponds to the N*C*-type superstructure with $N \geq 3$. Depending on the vacancy location, two sub-sites can exist (Fig. 8a): If the Fe–S–□ bond angle is near 129°, then the $(6J_1 + 12J_2 + 10J_3)$ couplings remain efficient. If the Fe–S–□ bond angle is near 62°, then all efficient couplings $(6J_1 + 12J_2 + 12J_3)$ are preserved. This site is similar to the Site-1.

(4) The Sites-4 appears when there are no vacancies in the selected Fe-layer, but the vacancies are located in two nearest layers both above and below the selected layer (Fig. 8b). In this case, all intralayer Fe–Fe and Fe–S–Fe bonds are preserved and the interlayer Fe–S–□ bonds appear in two neighboring layers. In this case vacancies may appear in each second iron layer along the *c*-axis, and this type of the vacancy ordering we attribute to the 2*C*-type superstructure.

Depending on the vacancy location, there are several types of the iron sites (see Fig. 8b) in which the Fe ion experiences the $(6J_1 + 12J_2 + 10J_3)$, $(6J_1 + 12J_2 + 11J_3)$ or $(6J_1 + 12J_2 + 8J_3)$ couplings with the nearest iron neighbors.

Thus, if all J_1, J_2, and J_3 interactions are taken into account, then the above considered interactions reduce to six nonequivalent Fe sites having the following exchange couplings:

$$\begin{aligned} \text{Site-A.1} &= (6J_1 + 12J_2 + 12J_3) \\ \text{Site-A.2} &= (5J_1 + 10J_2 + 12J_3) \\ \text{Site-A.3} &= (4J_1 + 8J_2 + 12J_3) \\ \text{Site-B} &= (6J_1 + 12J_2 + 11J_3) \\ \text{Site-C} &= (6J_1 + 12J_2 + 10J_3) \\ \text{Site-D} &= (6J_1 + 12J_2 + 8J_3) \end{aligned} \quad (1)$$

It was shown that the intralayer magnetic interactions, both the direct Fe–Fe and the 90° Fe–S–Fe superexchange one, are a good deal weaker than the interlayer superexchange Fe–S–Fe interactions, i.e., $J_3 \gg J_2 > J_1$ (Goodenough 1963; Hirahara and Murakami 1958; Motida and Miyahara 1970). Neglecting both the J_1 and J_2 interactions, only four nonequivalent Fe sites (with the $12J_3$, $11J_3$, $10J_3$, and $8J_3$ interactions) remain. We denote them as the Site-A($12J_3$), B($11J_3$), C($10J_3$), and D($8J_3$), respectively. As seen in Fig. 8, the A, B, and D sites maybe present with different probability in both the above mentioned superstructures N*C* with $N = 2$ and $N \geq 3$, while the D site with $8J_3$ interaction may not appear in the N*C* ($N \geq 3$) superstructures.

Based on the above analysis, we conclude that in our $Fe_{1-x}S$ nanoparticles, the values of the magnetic hyperfine fields H_{hf} about 335, 310, 279, and 245 kOe observed for four Mössbauer components at 80 K (see Table 2) correspond to the nonequivalent iron sites A, B, C, and D with the $12J_3$, $11J_3$, $10J_3$, and $8J_3$ exchange couplings, respectively. The corresponding room temperature values of H_{hf}, reduced to 300, 280, 260, and 232 kOe, are in a good agreement with the values of the fields for iron ions with 0, 1, 2, and 4 nearest vacancies, respectively, found in the bulk hexagonal $Fe_{0.909}S$ (the sites A, B, and C) and monoclinic $Fe_{0.881}S$ (the sites A, C, and D) compounds (Ovanesyan et al. 1971). The probability of appearance of different type vacancies in the $Fe_{1-x}S$ compounds depends on the vacancy concentration x and on the methods of synthesis. The presence of all four nonequivalent A, B, C, and D iron sites in our nanoparticles at $T < 300$ K implies a coexistence of two types of superstructures N*C* with $N = 2$ and $N \geq 3$.

The values of H_{hf} at nonequivalent iron sites, and the supertransferred hyperfine magnetic fields

The H_{hf} field values (of about 350–250 kOe) found in the sulfide $Fe_{1-x}S$ nanoparticles are much lower than

the typical values in iron oxides, which are about 550 kOe for Fe^{3+} ions in the octahedral oxygen coordination (Lyubutin 1969; Lyubutin et al. 1967a, b). This can be explained by different sources of the field in Fe $^{2+}$ and Fe^{3+} ions. The magnetic hyperfine field H_{hf} at iron nuclei is composed of three main contributions (Huang et al. 1966, 1967):

$$H_{hf} = H_c + H_{orb} + H_{STHF} \quad (2)$$

(i) The core term H_c appears from the core *s*-shells (of the own Fe ion) which are spin-polarized by the 3*d*-shell. It is so called the contact Fermi interaction (Watson and Freeman 1961). The H_c value in the Fe^{2+} ions is lower than that in the Fe^{3+} ions since the *d*-shell spin of Fe^{2+} ($S = 2$) is lower than in Fe^{3+} ($S = 5/2$).

(ii) The orbital field H_{orb} appears in Fe^{2+} from the own non-spherically symmetric $3d^6$-electron shell. This term is absent in the Fe^{3+} ions since the $3d^5$ shell is spherically symmetric and its orbital momentum is quenched. The sign of H_{orb} is opposite to the H_c term, thus the total H_{hf} field in Fe^{2+} is still more reduced.

(iii) The term H_{STHF} is so called "supertransferred hyperfine field" (STHF). In antiferromagnets, this field appears at Fe nuclei as a result of the transfer of spin density to the central cation Fe(↑) from neighboring cations having an opposite (antiparallel) spin Fe(↓) via superexchange Fe(↑)–L–Fe(↓), where L is the ligand. The mechanism of creation of the H_{STHF} field was first suggested by Huang et al. (1966, 1967) and further developed by others (Sawatsky and Van der Woude 1974; Van der Woude and Sawatsky 1971; Moskvin et al. 1977a, b; Lyubutin 1992).

The direction of the main field H_c is opposite to the iron 3*d* spin, i.e., the field H_c is negative with respect to the iron magnetization (Watson and Freeman 1961). On the contrary, the H_{orb} field is positive, and it reduces the total field value at iron nuclei. The direction of H_{STHF} coincides with the H_c direction increasing the total field H_{hf}.

In the nonequivalent iron sites of $Fe_{1-x}S$, the terms H_c and H_{orb} should be similar (at least, at low temperatures) but the H_{STHF} term depends on the number of nearest iron neighbors, and thus it is different for A, B, C, and D sites. Thus, from the Mössbauer data we can conclude that the highest field $H_{hf} = 335$ kOe (at 80 K) in our $Fe_{1-x}S$ nanoparticles corresponds to the Site-A($12J_3$) without any vacancies in the nearest neighboring. One vacancy decreases the field at the Site-B($11J_3$) by about 25 kOe; two vacancies reduce the field at the Site-C($10J_3$) by about 55 kOe, and four vacancies reduce the field at the Site-D($8J_3$) by 90 kOe. An average value of the H_{STHF} term in $Fe_{1-x}S$ can be estimated as (25 ± 3) kOe per one Fe–S–Fe superexchange bond at the angle of 129°.

In oxides, the value of H_{STHF} for Fe in the octahedral sites was evaluated as ~(10–20) kOe at 4.2 K (Lyubutin 1992; Abe et al. 1963; Petitt and Forester 1971; Boekema et al. 1979). It has been shown that the H_{STHF} values in the chalcogen compounds must be essentially higher than in oxides due to the strong covalent bonding between paramagnetic cation and chalcogen ligand (Lyubutin 1992; Lyubutin and Dmitrieva 1975; Okada et al. 1979; Dmitrieva et al. 2007).

Magnetic structure and magnetic sublattices

It is suggested that the magnetic structure of $Fe_{1-x}S$ consists of ferromagnetic iron layers which are antiferromagnetically coupled to each other along the *c*-axis (Bertaut 1953; Lotgering 1956; Marusak and Mulay 1979, 1980). The total magnetic moment M_{tot} appears from the competition between magnetic moments of neighboring layers, and the material can be AFM or FRM depending on the value of moments of the corresponding sublattices.

The Mössbauer measurements in the external magnetic fields revealed that in Fe_7S_8 (Levinson and Treves 1968), Fe_9S_{10} (Marusak and Mulay 1979, 1980), $Fe_{0.881}S$, and $Fe_{0.900}S$ (Ovanesyan et al. 1971) the direction of iron magnetic moments in the layers with vacancies (i.e., the site-A in our case) is opposite to the direction of moments in the layers without vacancies (i.e., the sites B, C, and D). Thus, the total magnetic moment M_{tot} of the compound appears as a result of the competition between magnetic moments M_A and $(M_B + M_C + M_D)$ of the corresponding magnetic sublattices. At room temperature the $(M_B + M_C + M_D)$ moment value is higher than the M_A moment, and M_{tot} is directed along the moments of the layers without vacancies.

$$\vec{M}_{tot} = \left(\vec{M}_B + \vec{M}_C + \vec{M}_D\right) - \vec{M}_A \quad (3)$$

Figure 9 shows the most probable ordering of the iron magnetic moments in layers with and without

vacancies alternating along the *c*-axis. The 2*C* type of the vacancy ordering shown in Fig. 9a provides a FRM state due to incomplete compensation of magnetic moments of the layers with and without vacancies. This type of magnetic structure is consistent with the Mössbauer data (Marusak and Mulay 1979, 1980; Levinson and Treves 1968). The AFM state appears in the 3*C* superstructure of Fig. 9b because of the complete compensation of the moments in layers with and without vacancies (by paired).

Vacancy redistribution

From the line areas of the Mössbauer components at 80 K we found that the occupation of the nonequivalent iron sites A, B, C, and D are in the ratio 1:1:1:0.5, respectively. At room temperature, the occupation of the C site slightly increases at the expense of the A and B sites. Heating the sample to the temperature 470 K, where maximum magnetization was observed in the magnetic measurements, reveals a considerable redistribution of the Mössbauer line areas. An essential increase in the occupations of the site-D was observed, while the occupation of the B site is reduced, and the occupation of the A and C sites remains almost unchanged. This shows an increase in the number of Fe ions with weaker exchange interactions $8J_3$ and the reduction of Fe ions with the $11J_3$ interaction.

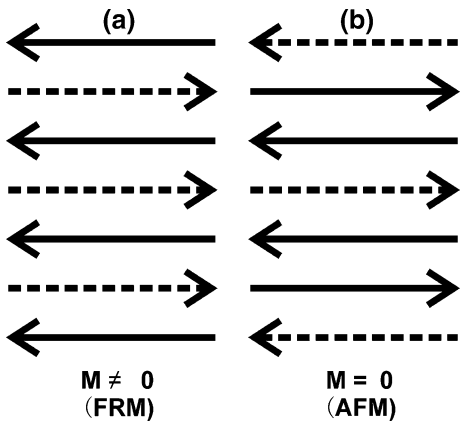

Fig. 9 Schematic view of the iron magnetic layers stacked along the *c*-axis in the NiAs-type crystal structure of $Fe_{1-x}S$ compound for the cases of 2*C*-type (**a**) and 3*C*-type (**b**) of the vacancy ordering. Directions of magnetization in the layers with vacancies (*dashed lines*) and without vacancies (*solid lines*) are shown by *arrows*. Ferrimagnetic structures (FRM), consistent with the Mössbauer observation, are realized in the (**a**) case, and antiferromagnetic (AFM) structure appears in the (**b**) case

The above analysis ("Nonequivalent iron sites" section) shows that Fe ions with $11J_3$ couplings at B-sites mainly exist in the superstructures where layers with vacancies are well separated from each other by two or more layers without vacancies (see Fig. 8a). We discern these type superstructures as N*C* type with $N \geq 3$. On the other hand, the D($8J_3$) sites may appear only in the superstructures where vacancies locate in every second iron layer along *c*-axis (Fig. 8b), and we discern these type of vacancy ordering as the 2*C* superstructure.

Thus, from the Mössbauer data we can conclude that upon heating the $Fe_{1-x}S$ nanoparticles to 470 K, the vacancy ordering changes from the N*C* ($N \geq 3$) type superstructure to the 2*C* type. As a result of vacancy redistribution, the AFM state (Fig. 9b) transforms to a FRM state (Fig. 9a), thus increasing the magnetization of the compound. In reality, as follows from the Mössbauer data, a mixture of both coexisting phases maybe present at all temperatures with different weights.

Above the Néel temperature ($T > 570$ K), the Mössbauer spectrum consists of a single doublet with broaden lines (Fig. 3). The nonequivalent iron sites are not detected in the paramagnetic temperature region. From the magnetic measurements, we found that upon subsequent cooling of the sample from 600 to 300 K the magnetization almost did not change and remains negligible (Fig. 6b). Meanwhile the Mössbauer spectrum, obtained at 300 K after heating the sample to 650 K, shows hyperfine magnetic spitting of the spectral lines typical of iron magnetic ordering. These data indicate that after heating above the Néel temperature, the material becomes a pure antiferromagnet and remains in that state down to 300 K. This effect can be explained by a random distribution of vacancies (over all iron layers) at high-temperatures which leads to the total compensation of the magnetic moments in neighboring layers. A single doublet with broaden lines in the Mössbauer spectrum at 650 K supports the random distribution of vacancies. The broaden lines associated with the random distribution of vacancies were also observed in several literature (Knodoro 1999; Kruse 1990; Knodoro and Kiwanga 1997).

It was found in the previous studies of the hexagonal pyrrhotites (Li and Franzen 1996) that

the value of magnetization measured in the cooling regime was higher than that at the sample heating. On the contrary, in our case the magnetization of heating branch is clearly higher than the cooling one. In the heating regime, a small increase of magnetization at temperatures above 400 K was recently observed in the $Fe_{0.92}S$ compound (Kim et al. 2009). This effect was explained by the rearrangement of vacancies but the Mössbauer data of the authors (Kim et al. 2009) show that the rearrangement starts at 570 K which is close to the Néel temperature. The peak-like transition behavior has been found in pyrrhotite group with composition Fe_9S_{10} which has a hexagonal closed-packed structure, and it was explained in terms of a vacancy rearrangement (Marusak and Mulay 1979, 1980).

Conclusion

The iron sulfide $Fe_{1-x}S$ nanoparticles with the shape of hexagonal plates or disks were successfully prepared by thermal decomposition method. At room temperature the compounds have the NiAs-type crystal structure. The Mössbauer spectroscopy and magnetic measurements data indicate that a mixture of AFM and FRM phases with the NC ($N \geq 3$) and 2C-type superstructures is present in the $Fe_{1-x}S$ compound at temperatures between 80 and T_N. At $T < 370$ K, the AFM phase prevails over the FRM phase. Upon the sample heating, the redistribution of iron vacancies at $T > 370$ K takes place and the vacancy ordering of the NC-type ($N \geq 3$) transforms to the ordering of the 2C-type which essentially increases the magnetization. Heating the sample above the Néel temperature 565 K leads to a random distribution of vacancies, and this state is quenched upon subsequent cooling of the sample to 300 K. This gives rise to a pure AFM structure with a zero magnetic moment due to the total compensation of the moments in neighboring iron layers. Thus, the high-temperature redistribution of cation vacancies leads to irreversible magnetic transitions in the $Fe_{1-x}S$ nanodisks. We believe that these interesting magnetic properties of the nanoparticles would find useful applications in technical devices.

Acknowledgments The authors thank Dr. D. Filimonov for his help in the high-temperature Mössbauer measurements. This study is supported by the Russian Academy of Sciences under the Program of Fundamental Research "Nanotechnology and Nanomaterials" (Grant no. 21-4.1.7) and by the Russian Foundation for Basic Research Grant #11-02-01464a. The authors also thank the National Science Council of Taiwan (NSC99-2112-M-218-001-MY3) for financial support.

References

Abe H, Matsuura M, Yasuoka H, Hirai A, Hashi T, Fukuyama T (1963) Nuclear magnetic resonance of Fe^{57} in nickel- and nickel-zinc-ferrites. J Phys Soc Jpn 18:1400–1406

Bertaut EF (1953) Contribution a l'étude des structures lacunaires: la pyrrhotine. Acta Crystallogr 6:557–561 (in French)

Boekema C, Jonker PC, Filoti G, Van der Woude F, Sawatsky GA (1979) Super transfer in doped $LaFeO_3$. Hyperfine Interact 7:45–60

Dmitrieva TV, Lyubutin IS, Stepin AS, Dubinskaya YuL, Smirnovskaya EM, Berry FJ, Thomas MF (2007) Diamagnetic nuclear probes Sn-119 in copper chromites $CuCr_2X_4$ (X = O, S, Se) with spinel structure. JETP 104:554–561 (in English) [Zh Eksp Teor Fiz (2007) 131:624–633 (in Russian)]

Fei YW, Prewitt CT, Mao HK, Bertka CM (1995) Structure and density of FeS at high pressure and high temperature and the internal structure of Mars. Science 268:1892–1894

Goodenough JB (1963) Magnetism and the chemical bonds. Interscience, New York

Hirahara E, Murakami M (1958) Magnetic and electrical anisotropies of iron sulfide single crystals. J Phys Chem Solids 7:281–289

Huang NL, Orbach R, Simanek E (1966) Contribution to the hyperfine field from cation-cation interactions. Phys Rev Lett 17:134–136

Huang NL, Orbach R, Simanek E, Owen J, Taylor DR (1967) Cation-cation interaction contributions to the hyperfine interaction. The "supertransferred hyperfine interaction". Phys Rev 156:383–390

Kim W, Park IJ, Kim CS (2009) Mössbauer study of magnetic structure of cation-deficient iron sulfide $Fe_{0.92}S$. J Appl Phys 105:07D535(1–3)

Knodoro JWA (1999) Mössbauer study of vacancies in natural pyrrhotite. J Alloys Compd 289:36–41

Knodoro JWA, Kiwanga CA (1997) Mössbauer study of natural pyrrhotites. Appl Radiat Isot 48:555–563

Kruse O (1990) Mössbauer and X-ray study of the effects of vacancy concentration in synthetic hexagonal pyrrhotites. Am Mineral 75:755–763

Langford JI, Wilson AJC (1978) Scherrer after sixty years: a survey and some new results in the determination of crystallite size. J Appl Crystallogr 11:102–113

Levinson LM, Treves D (1968) Mössbauer study of the magnetic structure of Fe_7S_8. J Phys Chem Solids 29: 2227–2231

Li F, Franzen HF (1996) Ordering, incommensuration, and phase transitions in pyrrhotite, part II: a high-temperature X-ray powder diffraction and thermomagnetic study. J Solid State Chem 126:108–120

Lin CR, Siao YJ, Lu SZ, Gau C (2009) Magnetic properties of iron selenide nanocrystals synthesized by the thermal decomposition. IEEE Trans Magn 45:4275–4278

Lin CR, Lu SZ, Lyubutin IS, Korzhetskiy YV, Wang SC, Suzdalev IP (2010) Synthesis and magnetic properties of iron sulfide nanosheets with a NiAs-like structure. J Appl Phys107:09A335(1–3)

Lotgering FK (1956) Ferrimagnetism of sulfides and oxides I. The iron-sulfur system. Philips Res Rep 11:190–217

Lyubutin IS (1969) Magnetism and crystal chemistry of iron garnets studied by Mössbauer spectroscopy (review). In: Proceedings of the international conference on the applications of the Mössbauer effect, Tihany, Hungary, pp 467–489

Lyubutin IS (1992) The technique of the diamagnetic nuclear probe in investigations of magnetic properties of crystals. Physical crystallography, series: problems of the modern crystallography. Nauka Publishers, Moscow, pp 326–363 (in Russian)

Lyubutin IS, Dmitrieva TV (1975) Strong supertransferred magnetic fields at nuclei of diamagnetic tin atoms in chalcogenide spinels. JETP Lett 21:59–62 (in English) [Pis'ma Zh Eksp Teor Fiz 21:132–135 (in Russian)]

Lyubutin IS, Makarov EF, Povitskii VA (1967a) Magnetic and electric hyperfine interactions of Fe-57 nuclei in $Y_{3-x}Ca_xFe_{5-x}Sn_xO_{12}$ compounds. J Symp Faraday Soc 1: 31–41

Lyubutin IS, Makarov EF, Povitskii VA (1967b) Mossbauer effect at Fe-57 nuclei in $Y_{3-x}Ca_xFe_{5-x}Sn_xO_{12}$ compounds with $0<x<2$. Sov Phys JETP 26:44–57 (in English) [Zh Eksp Teor Fiz (1967) 53:65–78 (in Russian)]

Marusak LA, Mulay LN (1979) Mössbauer and magnetic study of the antiferro to ferrimagnetic phase transition in Fe_9S_{10} and the magnetokinetics of the diffusion of iron atoms during the transition. J Appl Phys 50:1865–1867

Marusak LA, Mulay LN (1980) Polytypism in the cation-deficient iron sulfide, Fe_9S_{10}, and the magnetokinetics of the diffusion process at temperatures about the antiferro- to ferrimagnetic (λ) phase transition. Phys Rev B 21: 238–244

Moskvin AS, Ovanesyan NS, Trukhtanov VA (1977a) Supertransferred hyperfine interaction in magnetic insulators (I). Theoretical considerations. Hyperfine Interact 3:429–447

Moskvin AS, Ovanesyan NS, Trukhtanov VA (1977b) Supertransferred hyperfine interaction in magnetic insulators (II). Perovskite-like structures. Hyperfine Interact 5:13–26

Motida K, Miyahara S (1970) On the 90° exchange interaction between cations (Cr^{3+}, Mn^{2+}, Fe^{3+} and Ni^{2+}) in oxides. J Phys Soc Jpn 28:1188–1196

Nakazawa H, Morimoto N (1971) Phase relations and superstructures of pyrrhotite, $Fe_{1-x}S$. Mater Res Bull 6: 345–358

Ok HN, Lee SW (1973) Mössbauer study of ferrimagnetic Fe_7Se_8. Phys Rev B 8:4267–4269

Ok HN, Lee CS (1984) Mössbauer study of FeV_2Se_4. Phys Rev B 29:5168–5170

Ok HN, Baek KS, Kim CS (1982) Crystallographic and Mössbauer studies of $FeRh_2Se_4$. Phys Rev B 26:4436–4441

Okada T, Sekizawa H, Yamadaya T (1979) Hyperfine interaction of ^{119}Sn in magnetic chalcogen spinels. J Phys 40-C2:299–300

Ovanesyan NS, Trukhtanov VA, Odinets GY, Novikov GV (1971) Vacancy distribution and magnetic ordering in iron sulfides. Sov Phys JETP 33:1193–1202 (in English) [Zh Eksp Teor Fiz (1971) 60:2220–2229 (in Russian)]

Petitt GA, Forester DW (1971) Mössbauer study of cobalt-zinc ferrites. Phys Rev B 4:3912–3923

Rusakov VS (2000) Mössbauer spectroscopy of locally heterogeneous systems [Messbauerovskaya spektroskopiya lokal'no neodnorodnykh sistem]. Nuclear Physics Institute, Almaty (in Russian)

Sawatsky GA, Van der Woude F (1974) Covalency effects in hyperfine interactions. J Phys 35-C6:47–60

Takayama T, Takagi H (2006) Phase-change magnetic memory effect in cation-deficient iron sulfide $Fe_{1-x}S$. Appl Phys Lett 88:012512(1–3)

Van der Woude F, Sawatsky GA (1971) Hyperfine magnetic fields at Fe^{57} nuclei in ferrimagnetic spinels. Phys Rev B 4:3159–3165

Wang H, Salveson I (2005) A review on the mineral chemistry of the non-stoichiometric iron sulphide, $Fe_{1-x}S$ ($0 \leq x \leq 0.125$): polymorphs, phase relations and transitions, electronic and magnetic structures. Phase Transitions 78: 547–567

Watson RE, Freeman AJ (1961) Origin of effective fields in magnetic materials. Phys Rev 123:2027–2047

Wolf A, Dwight K (1993) Solid state chemistry: synthesis, structure, and properties of selected oxides and sulfides. Chapman & Hall, Inc, New York

Zapletal K (1969) Connection of some magnetic properties with the phase composition of natural pyrrhotites. Stud Geophys Geod 13:191–198